Atmospheric
Chemistry
and Physics

Investigating types and sources of organic aerosol in Rocky Mountain National Park using aerosol mass spectrometry

M. I. Schurman[1], **T. Lee**[1,*], **Y. Sun**[1,**], **B. A. Schichtel**[2], **S. M. Kreidenweis**[1], **and J. L. Collett Jr.**[1]

[1]Department of Atmospheric Science, Colorado State University, Fort Collins, CO, USA
[2]National Park Service/CIRA, Colorado State University, Fort Collins, CO, USA
[*]now at: Department of Environmental Science, Hankuk University of Foreign Studies, Seoul, South Korea
[**]now at: State Key Laboratory of Atmospheric Boundary Layer Physics and Atmospheric Chemistry, Institute of Atmospheric Physics, Chinese Academy of Sciences, Beijing, China

Correspondence to: M. I. Schurman (mishaschurman.ms@gmail.com)

Abstract. The environmental impacts of atmospheric particles are highlighted in remote areas where visibility and ecosystem health can be degraded by even relatively low particle concentrations. Submicron particle size, composition, and source apportionment were explored at Rocky Mountain National Park using a High-Resolution Time-of-Flight Aerosol Mass Spectrometer. This summer campaign found low average, but variable, particulate mass (PM) concentrations (max $= 93.1\,\mu g\,m^{-3}$, avg. $= 5.13 \pm 2.72\,\mu g\,m^{-3}$) of which $75.2 \pm 11.1\,\%$ is organic. Low-volatility oxidized organic aerosol (LV-OOA, 39.3 % of PM_1 on average) identified using Positive Matrix Factorization appears to be mixed with ammonium sulfate (3.9 % and 16.6 % of mass, respectively), while semi-volatile OOA (27.6 %) is correlated with ammonium nitrate (nitrate: 4.3 %); concentrations of these mixtures are enhanced with upslope (SE) surface winds from the densely populated Front Range area, indicating the importance of transport. A local biomass burning organic aerosol (BBOA, 8.4 %) source is suggested by mass spectral cellulose combustion markers (m/z 60 and 73) limited to brief, high-concentration, polydisperse events (suggesting fresh combustion), a diurnal maximum at 22:00 local standard time when campfires were set at adjacent summer camps, and association with surface winds consistent with local campfire locations. The particle characteristics determined here represent typical summertime conditions at the Rocky Mountain site based on comparison to ∼10 years of meteorological, particle composition, and fire data.

1 Introduction

From alpine meadows to stark peaks, Rocky Mountain National Park (RMNP) hosts abundant wildlife, an important water catchment, and roughly 3 million visitors per year (Annual Park Visitation Report, NPS Public Use Statistics Office). Recent studies chronicle visibility reduction in RMNP, a Clean Air Act Class I protected environment, due to fine particles, especially in the summer when concentrations are higher (Levin et al., 2009; Malm et al., 2009b). Environmental impacts from increased nutrient – and particularly nitrogen – deposition are also documented in the Colorado Rocky Mountains (Baron et al., 2000), where mountain–valley circulations periodically transport ammonium, nitrate, and other particulate species from agricultural and urban sources to the east (Benedict et al., 2013a, b). However, organic compounds contribute the majority of fine-particle mass and attendant visibility impairment at RMNP during summer months (average July 1991–2006 $PM_{2.5}$ organic mass fraction $= 51 \pm 6\,\%$, Levin et al., 2009); unfortunately, beyond indications that contemporary carbon (denoting biomass burning and/or biogenic volatile organic carbon (VOC) condensation) and organic nitrogen contribute to organic mass (Benedict et al., 2013a; Schichtel et al., 2008), local organic aerosol (OA) types and sources are unknown. In fact, studies concerning remote environments are infrequent despite the myriad health, environmental, and climate effects of fine particles (Solomon et al., 2007) and the fact that such sites comprise the atmospheric "background" that contextu-

alizes our developing understanding of atmospheric chemistry. Those that do exist indicate a range of particle sources from transported urban particles (e.g., Sun et al., 2009) to biomass burning (e.g., Corrigan et al., 2013) and secondary OA formation involving biogenic VOCs (e.g., Chen et al., 2009); efficient mitigation strategies clearly require a sophisticated understanding of OA sources.

This study explores particle sources and composition at a remote site in RMNP from 2 July to 31 August 2010 as part of the Rocky Mountain Atmospheric Nitrogen and Sulfur (RoMANS) Study. The Aerodyne Time-of-Flight Aerosol Mass Spectrometer (HR-ToF_AMS or AMS)) analyzes submicron, non-refractory particles quantitatively for size and composition with high mass and time resolution (Decarlo et al., 2006); Positive Matrix Factorization (PMF) is used to deconvolve a matrix containing 2–5 min average organic mass spectra into a number of spectrally static organic "factors" whose contributions to total organic mass vary over time (Paatero and Tapper, 1994).

PMF-derived factor mass spectra (MS) may reveal particle sources through comparison with MS profiles of various compounds and aerosol types (Alfarra et al., 2007; Lanz et al., 2007; Zhang et al., 2011). Correlating factors with inorganic tracers by particle size and concentration may also support source identification (Zhou et al., 2005). For instance, biomass burning organic aerosol (BBOA) may be identified by fragments of levoglucosan ($C_6H_{10}O_5$) and other anhydrosugars – products of cellulose and hemicellulose combustion – in the ambient mass spectra at m/z 60 ($C_2H_4O_2+$), m/z 73 ($C_3H_5O_2+$), etc. (Simoneit et al., 1999; Weimer et al., 2008); BBOA is sometimes, but not always, correlated with potassium (K), another known combustion tracer (Echalar et al., 1995; Sullivan et al., 2008).

Other common classifications are based on organic compounds' degrees of oxidation. Hydrocarbon-like organic aerosol (HOA) is produced chiefly by fuel combustion and distinguished by hydrocarbon chains at m/z 57 ($C_4H_9^+$; Lanz et al., 2007; Zhang et al., 2005). The spectrum of semi-volatile oxidized organic aerosol (SV-OOA or OOA-II) is characterized by the predominance of hydrocarbons and/or carbonyls at m/z 43 ($C_3H_7^+$ or CH_3CO^+) over more oxidized fragments at m/z 44 (mostly CO_2^+; Lanz et al., 2007; Ulbrich et al., 2009). Lastly, enhanced signal at m/z 44 indicates highly oxidized low-volatility oxidized organic aerosol (LV-OOA or OOA-I; Lanz et al., 2007; Ulbrich et al., 2009); OOA is often observed in rural and remote areas (Zhang et al., 2007). Using particle composition with factor analysis, particle size, and meteorological data, this work constructs a comprehensive description of submicron particle sources and suggests, through comparison to historical data, that these represent "typical" summer conditions at Rocky Mountain National Park.

2 Methods

Particles were sampled in a valley on the SE side of Rocky Mountain National Park at ∼2740 m (lat: 40.2778, long: 105.5453; Fig. 1). The sampling site is adjacent to the Salvation Army High Peak, Covenant Heights, Timberline, and Aspen Lodge Resort camps, but removed from urban centers and considered rural; traffic on the nearby Colorado Hwy 7 is light. The AMS was co-located with meteorological, CAST-Net, and IMPROVE (designator: ROMO) stations, a particle-into-liquid sampler (PILS-IC; Orsini et al., 2003), high-volume filter samplers, URG annular denuders, a differential mobility particle sizer (DMPS; TSI 3085), an optical particle counter, an aerodynamic particle sizer, and an automated precipitation sampler. Beem et al. (2010), Levin et al. (2009), and Benedict et al. (2012) present results from measurements using some of the above instrumentation. Rigorous AMS calibration and data quality assurance protocols were used, including weekly or bi-weekly ionization efficiency calibrations and HEPA filtration periods. Data analysis utilized SQUIRREL (v1.51H), PIKA (v1.10H; DeCarlo et al., 2006), and the PMF2 algorithm (Paatero and Tapper, 1994) in PET (v2.03A; Ulbrich et al., 2009) in Igor Pro 6.22A (Wave-Metrics Inc., Lake Oswego, OR). Elemental analysis of high-resolution mass spectra utilized the updated AMS fragmentation table for ambient OA in Aiken et al. (2008). Data preparation for the PMF analysis followed Zhang et al. (2011) and Ulbrich et al. (2009) and included fragments m/z 12–110; solutions for one to five factors were explored with varying rotational parameters ($-1 \leq$ FPEAK ≤ 1, in increments of 0.2). A three-factor solution was selected based on criteria presented in Ulbrich et al. (2009) and Zhang et al. (2011); diagnostic information for this PMF solution can be found in the supplement, along with two- and four-factor solutions (Figs. S1, S4, and S5 in the Supplement).

The selection of number of PMF factors is based on factors' spectral and timeline dissimilarities (Fig. S1b in the Supplement), comparison to "established" factor types, and correlation with tracers such as anthropogenic inorganic species concentrations (Zhang et al., 2011; Ulbrich et al., 2012); factor number choice may be supported using Q (a parameter describing residuals) and other statistics. Q is defined as (Paatero et al., 2002):

$$Q = \sum_i \sum_j (e_{ij} / \sigma_{ij})^2,$$

where e is residual, not fit by the algorithm and σ is the estimated error over all rows (i, MS fragments) and columns (j, time) of the data and corresponding error matrices. For the Rocky Mountain study, a three-factor solution is supported by a large (36 %) reduction in Q between two- and three-factor solutions, indicating that the three-factor solution describes considerably more of the variability in the data set, but diminishing reduction (≤ 21 %) in Q when four or more factors are chosen (Fig. S1c in the Supplement). A
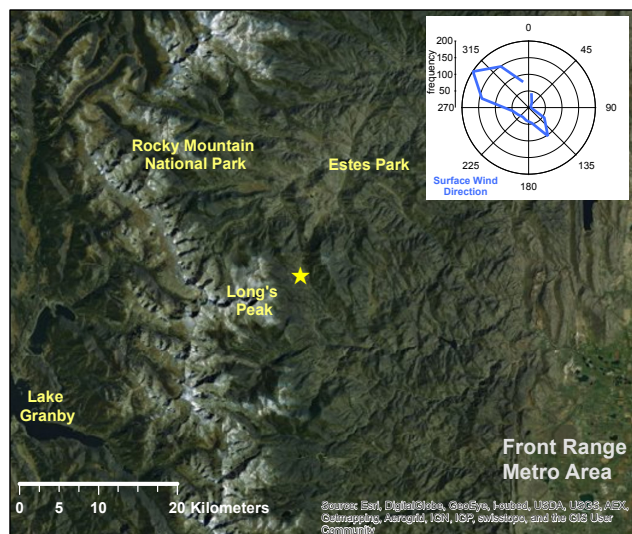
Figure 1. Map showing the Rocky Mountain National Park sampling site (yellow star). Boulder, Denver, and other cities form the Front Range metro area to the east (ARCgis map generation: Zitely Tzompa, 15 March 2014). The wind rose shows a histogram of wind directions measurements during the study.

Figure 2. Study-average diurnal variation of ambient temperature (red dashed line, left axis) and surface wind direction (blue line, right axis).

second variable, Q_{exp}, equals the degrees of freedom (for AMS data, approximately the number of data points in the input data matrix) and $Q / Q_{exp} = 0.08$ for this data set (Ulbrich et al., 2009; Paatero and Tapper 1993). As described in the literature, $Q / Q_{exp} \ll 1$ indicates an overestimation of error (Paatero et al., 2002; Ulbrich et al., 2009). Error determination for the error matrix input to PMF involves the data collection averaging time and the standard deviation of the single-ion area, both determined by the data acquisition software (Allan et al., 2003). We hypothesized that the low total signal (due to low mass) could contribute to reduced signal-to-noise ratio overall, putting a larger percentage of data points (fragment mass at a given time) under the signal-to-noise ($S : N = sqrt(\sum signal^2 / \sum err^2)$) threshold that recommends down-weighting (increasing the error) during error matrix preparation; points with $S : N < 0.2$ ("bad") are excluded from the analysis and those with $0.2 < S : N < 2$ ("weak") are down-weighted by a factor of 2 (Paatero and Hopke, 2003). All "bad" fragments were evaluated individually and featured time series dominated by noise, and thus their exclusion was sustained. The down-weighting factor for weak fragments was subsequently reduced to 1.2, resulting in $Q / Q_{exp} = 0.1$ for a three-factor solution. The Q / Q_{exp} improvement is minimal and the ensuing factors are nearly identical to those here, so the original analysis (down-weight factor of 2) was used. Although the source of the error overestimation was not determined, residual mass between measured values and the PMF reconstruction is low and fairly constant over time (Fig. S1f and g in the Supplement); also, the histogram of scaled residuals for each m/z indicates that
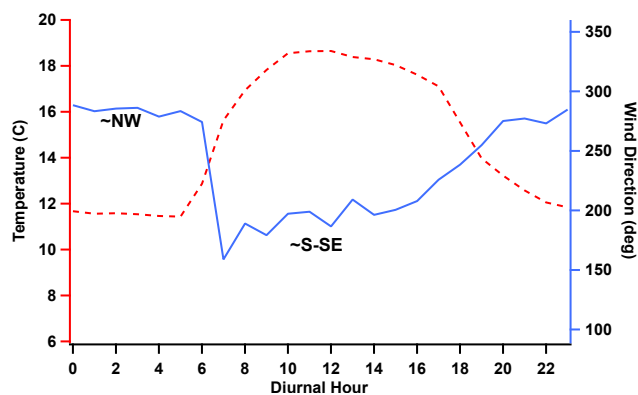
though the PMF reconstruction of mass tends slightly too low, this bias is consistent across m/z and thus should have little effect on the interpretation of results (Fig. S1d). The PMF analysis was repeated twice from HR fragment selection onward and twice with different error constraints with very similar results.

Chemical source apportionment is often supported by meteorological information; many studies have used wind direction, HYSPLIT, and other back-trajectory products to map source regions and transport (Chan et al., 2011; Sun et al., 2010). Here, complex flow over mountainous terrain produces back trajectories that may be useful in aggregate but lack the specificity needed to study individual events (Gebhart et al., 2011); fortunately, links between increased NO_x concentrations and low-level upslope flow from the Front Range indicate that less complex meteorological analysis may aid source apportionment (Parrish et al., 1990). Thermally induced afternoon upslope (NE–S, 45–180°) and nighttime downslope (SW–N, 225–360°) winds are well established in the Rocky Mountains and may transport urban plumes toward or away from the RMNP site, respectively (Figs. 1 and 2 in Bossert and Cotton, 1994); the co-located ROMO met station records hourly surface observations.

The conditional probability function (CPF) identifies wind directions contributing high constituent concentrations and is well supported in the literature (Kim and Hopke, 2004; Xie and Berkowitz, 2007); the CPF equals the number of concentration points greater than a threshold (here, the concentration average plus one standard deviation) measured in a given wind sector divided by the number of data points in that sector.
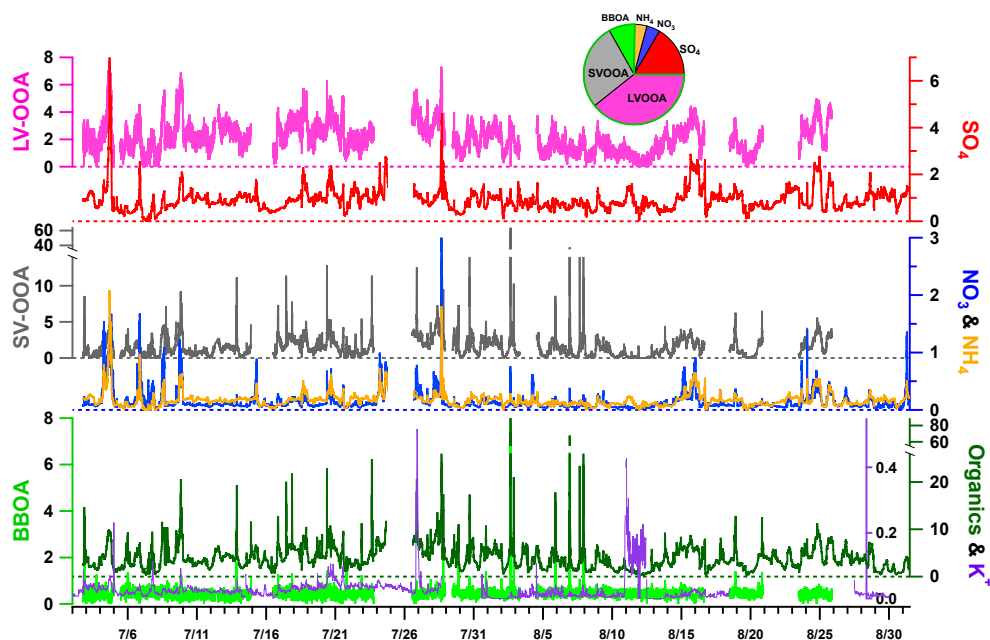
Figure 3. Time series of inorganic components, total organics, and organic factors (LV-OOA, SV-OOA, and BBOA) in µg m^{-3}. Potassium (K$^+$) is from 17 min average PILS-IC samples. The pie chart shows study-average contributions for each component; the dark green outline contains total organics.

3 Results

3.1 General particle composition and concentration

Submicron aerosol mass concentrations during these summer measurements were fairly low, with an average (± 1 SD) of 5.13 ± 2.72 µg m^{-3}, and comparable to average PM$_{2.5}$ measurements from the IMPROVE network during July and August from 2005 to 2012 (5.13 ± 4.36 µg m^{-3}; CIRA, 2013). Total organics dominate with frequent higher-concentration events manifested in both brief, high-amplitude spikes and longer-duration, lower-intensity increases (max $= 93.1$ µg m^{-3}, avg. 3.86 ± 2.66 µg m^{-3}; Fig. 3); organics contribute 75.2 ± 11.1 % of total non-refractory submicron mass on average, which is consistent with the organic contribution to 24 h average PM$_{2.5}$ found in the summer of 2006 (60 ± 12 %; Hand et al., 2012; Levin et al., 2009). Sulfate concentrations are lower and less variable (max $= 7.45$ µg m^{-3}, avg. 0.85 ± 0.48 µg m^{-3}); nitrate and ammonium concentrations are also low on average but with some higher concentration episodes (Fig. 3; NO$_3$: max $= 5.37$ µg m^{-3}, avg. 0.22 ± 0.24 µg m^{-3}; NH$_4$: max. $= 2.05$ µg m^{-3}, avg. 0.20 ± 0.14 µg m^{-3}). These values are statistically similar to concentrations in previous data sets covering 2005–2012, showing low inter-annual variability in major species and total particulate mass (Table 1). Time series correlations indicate ammonium nitrate ($r^2 = 0.89$) and ammonium sulfate ($r^2 = 0.97$) mixtures; ammonium nitrate and ammonium sulfate commonly arise in ambient parti-

cles produced from ageing of agricultural, industrial, and other anthropogenic sources. The low correlation between nitrate and sulfate ($r^2 = 0.34$; Table 2) may indicate that they are not regularly internally mixed in the local aerosol. Formation mechanisms and/or upwind source types and locations for particulate ammonium nitrate and ammonium sulfate may differ: ammonium nitrate may arise from reaction of gaseous nitric acid and ammonia, while the presence of sulfate may reflect in-cloud or gas phase oxidation of sulfur dioxide (Barth et al., 2000; Lelieveld and Heintzenberg, 1992; Seinfeld and Pandis, 2006); this will be explored further in following sections.

Diurnal average concentration patterns are shown in Fig. 4. Nighttime increases in inorganics may be caused by thermal partitioning and/or boundary layer compression and mirror those seen in OOA PMF factors, as discussed later. Diurnal means of inorganic species increase sharply in the afternoon in contrast to the 25th and 75th percentiles, which are similar in profile to the oxidized organics (next section); this indicates that the mean values are influenced disproportionately by fewer, high-concentration events and may not indicate "typical" behavior. The afternoon increases in the means of sulfate and ammonium have a pattern different than that of nitrate, supporting the suggestion that events and/or mechanisms driving concentrations of ammonium sulfate differ from those influencing nitrate. Nitrate has a bi-modal mean similar to total organics and presaging the organic nitrogen content explored in Sect. 3.3. Concentrations of inorganic species and total organics begin to increase at $\sim$10:00–

Table 1. July–August average ± standard deviation concentrations of particulate species in µg m^{-3}. The IMPROVE network collects 24 h PM$_{2.5}$ nylon-filter samples for nitrite, nitrate, sulfate, and chloride, and quartz filters for organic matter and elemental carbon analysis. IMPROVE data are averaged over July and August during 2005–2012 ("IMPROVE") or over July and August during 2010 ("IMPRV 2010"), and were accessed via the VIEWS database on 22 January 2014. Bold text indicates significant difference (using Wilcoxon Rank test) between IMPROVE 2010 and AMS data averaged to the 24 h IMPROVE time resolution. * Benedict et al. (2013). ** IMPROVE does not measure ammonium; it is calculated as the amount needed to neutralize sulfate and nitrate.

	NO$_3$	SO$_4$	NH$_4$	OM	PM$_{2.5}$
This study	0.22 ± 0.24	0.85 ± 0.48	0.20 ± 0.14	3.86 ± 2.66	PM$_1$: 5.13 ± 2.72
Summer 2006*	0.12	0.99	0.32		
Summer 2010*	0.08 ± 0.06	0.31 ± 0.14	0.18 ± 0.07		
IMPROVE	0.08 ± 0.10	0.42 ± 0.19	0.02 ± 0.03**	3.90 ± 6.11	5.13 ± 4.36
IMPRV 2010	**0.12 ± 0.13**	**0.53 ± 0.27**	**0.04 ± 0.04****	**1.48 ± 0.64**	**3.13 ± 1.29**

Table 2. Time-series coefficients of determination (r^2) calculated using the IGOR linear regression algorithm between inorganic species, organic factors from the original PMF solution, and (*) organic factors from the six-factor recombination.

	LVOOA	SVOOA	BBOA	SO$_4$	NO$_3$	LVOOA*	SVOOA*	BBOA*
SO$_4$	0.77	0.18	0.05			0.44	0.30	0.02
NO$_3$	0.33	0.41	0.02	0.34		0.32	0.33	0.07
NH$_4$	0.76	0.72	0.03	0.97	0.89	0.50	0.34	0.03
SVOOA*						0.56		
BBOA*						0.08	0.16	

12:00 LST, approximately 2–4 h after the ∼08:00 LST initiation of upslope winds (Fig. 2), consistent with typical lags observed in episode analysis (Sect. 3.7).

3.2 PMF-derived organic aerosol factors

The selection of number of PMF factors is based on factors' spectral and timeline dissimilarities, comparison to "established" factor types, and correlation with tracers such as inorganic species. Positive matrix factorization suggests a three-factor solution with biomass burning organic aerosol (BBOA, Fig. 5; Simoneit et al., 1999) and two types of oxidized organics: low-volatility oxidized organic aerosol (LV-OOA) and semi-volatile oxidized organic aerosol (SV-OOA; Lanz et al., 2007; Ng et al., 2010), as defined in the introduction. All of these factors are quite oxidized, with oxygenated fragments often dominating signal at a given m/z (note fragment families C$_x$H$_y$O$_1$ and C$_x$H$_y$O$_{n>1}$ in Fig. 5) and significant CH$_3$CO$^+$ (at m/z 43) and CO$_2^+$ (at m/z 44).

PMF solutions are subjective since they involve qualitative user inputs such as number of factors; indeed, we hypothesize that some BBOA mass may be misallocated to the SV-OOA factor by the algorithm. The most compelling evidence is that the SV-OOA mass spectrum contains some m/z 60 and m/z 73, but average mass spectra of all high-SV-OOA periods with no commensurate increase in BBOA do not contain mass at m/z 60 and 73 (Fig. S3 in the Supplement); therefore, an SV-OOA mass spectrum containing
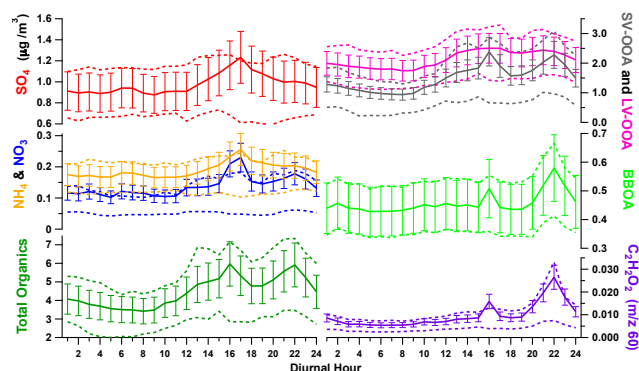

Figure 4. Study-average diurnal concentrations of particulate sulfate, nitrate, ammonium, total organics, BBOA, LV-OOA, SV-OOA, C$_3$H$_3$O$^+$ (m/z 55), and C$_2$H$_4$O$_2^+$ (m/z 60, levoglucosan). Solid lines are means, with ± 20 % error bars reflecting AMS quantitation error. Dashed lines are 25th and 75th percentiles.

these biomass burning markers does not represent the vast majority of elevated-SV-OOA periods.

Secondly, timeline and meteorological data indicate that the OOA factors are transported with inorganics from the Front Range (Sect. 3.5); dilution during transport tends to yield gradual, sustained, and moderate (∼2–3 times average) concentration increases (Fig. 3). The appearance, then, of brief, high-amplitude SV-OOA events commensurate with BBOA but not with inorganics is inconsistent with the likely behavior of transported, aged SV-OOA (see example: period
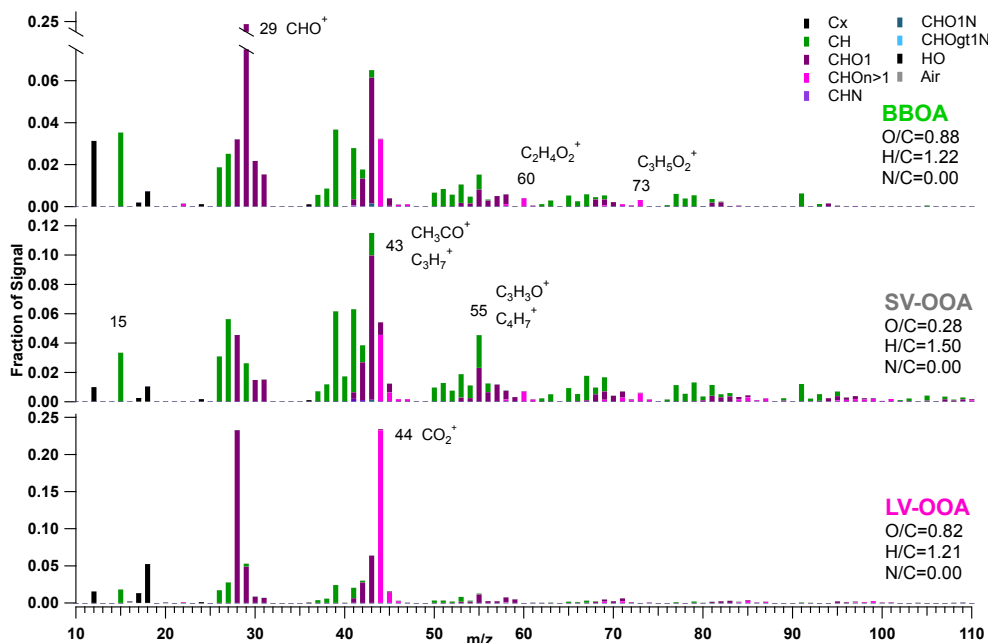
Figure 5. Normalized mass spectra of organic aerosol types determined by positive matrix factorization (Paatero and Tapper, 1994): biomass burning organic aerosol (BBOA), semi-volatile oxidized organic aerosol (SV-OOA), and low volatility oxidized organic aerosol (LV-OOA). Elemental ratios are calculated for the given factor mass spectrum.

A, Fig. 12). This is not conclusive, of course, as real increases in particulate SV-OOA could also arise from semivolatile organic carbon condensation onto the newly available biomass burning particle surface area. However, diurnal patterns echo these timeline idiosyncrasies; the 22:00 LST increase in BBOA is mirrored in the diurnal modes of m/z 60 and SV-OOA (Fig. 4), but in a PMF run excluding periods with BBOA events (defined as $f60 > 0.003$, the ambient background), SV-OOA increases only slightly at night and is similar to LV-OOA in amplitude and pattern (Fig. S3). Apportionment of some BBOA mass to SV-OOA would account for enhanced m/z 60 mass in the SV-OOA mass spectrum and the increased SV-OOA concentration during BBOA events.

In PMF, the FPEAK parameter is used to explore linear transformations, or "rotations", of the solution matrix that redistribute mass between the factors, presenting alternate solutions (Ulbrich et al., 2009). Positive FPEAK allocates less m/z 60 and 73 to SV-OOA and more to BBOA, but also reallots mass at other m/z to BBOA; this renders the BBOA timeline increasingly like that of SV-OOA, which is unphysical because it suggests that BBOA increases during periods when no biomass burning markers are present in the mass spectra, as explained above. A six-factor solution with subsequent recombination to three factors produced better-resolved BBOA and SV-OOA factors, for which increases in $f60$ are commensurate with increases in BBOA but not with SV-OOA (Fig. 6). The six factors were recombined based on timeline similarity (see Fig. S2 in the Supplement) such that *BBOA = Factor 5 + Factor 6, *SV-OOA = Factor 3

+ Factor 4, and *LV-OOA = Factor 1 + Factor 2; Table 2 shows coefficients of determination (r^2) between the mass spectral profiles of the recombinant solutions. This solution produced the conclusions, as above, that LV-OOA is associated with ammonium sulfate, SV-OOA is associated with ammonium nitrate, and BBOA has sporadic, high amplitude events (Table 2). However, since this recombination technique is more subjective and yields the same conclusions about the local aerosol, the original three-factor PMF analysis with FPEAK = 0 is presented here.

The LV-OOA factor is generally most abundant (average = $2.15 \pm 1.11\,\mu g\,m^{-3}$) and features longer duration ($\sim$6–11 h), low amplitude (2–3 times average) elevated-concentration events. The LV-OOA time series is correlated with sulfate and ammonium (Table 2), similar to studies with LV-OOA factors from anthropogenically influenced secondary aerosol formation (Zhang et al., 2011). Internal mixing of sulfate and low-volatility OA may arise from similar oxidation pathways; the advanced oxidative processing that produces low-volatility OA will also tend to produce S(VI) if S(IV) species are present in the same air mass (Jimenez et al., 2009). For instance, aqueous processing is known to efficiently produce both low-volatility organic compounds and S(VI) species.

The LV-OOA factor increases consistently in the afternoon (diurnal mean mode at 14:00–15:00 LST) and nighttime (mode at 22:00 LST, Fig. 4). The afternoon increase may arise from transport with upslope winds, as will be explored later; the nighttime concentration maximum begins
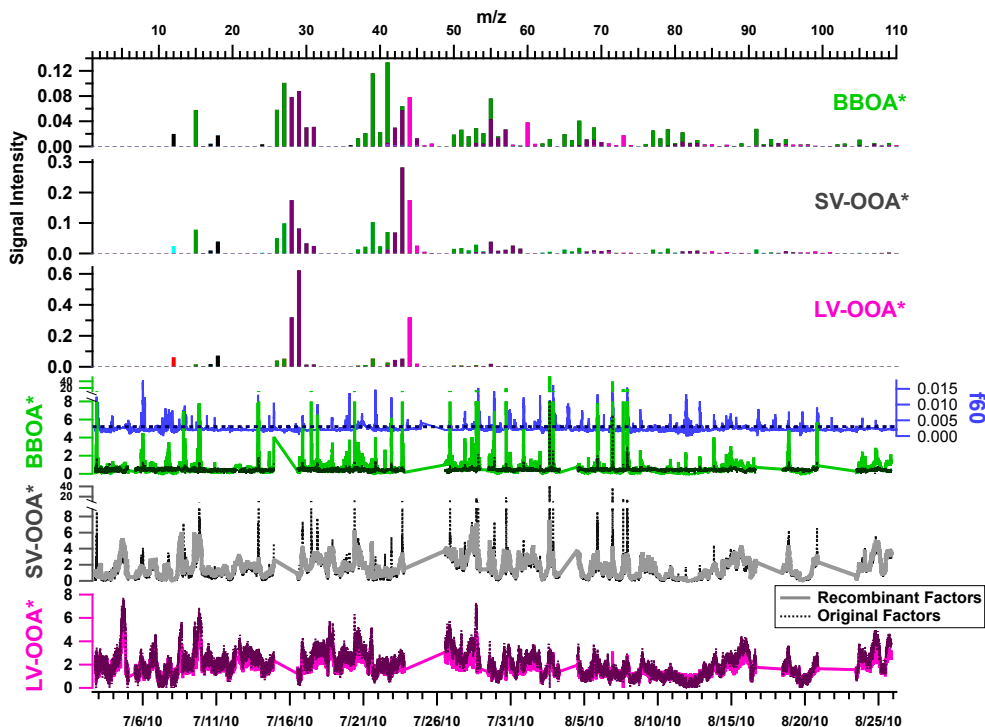
Figure 6. (Top) Factor mass spectra for the six-factor recombination, and (bottom) timelines of LV-OOA, SV-OOA, and BBOA from the original three-factor PMF solution and the six-factor recombination, with *f60* (right axis; the ambient *f60* background value (0.003), above which biomass burning is indicated, is denoted by the dashed blue line).

to form at ∼16:00 LST, when temperatures start to drop (Fig. 2), which may indicate effects from boundary layer compression and/or thermal partitioning. Both OOA factors also feature a subtle 08:00 LST minimum, which could be attributed to thermal boundary layer expansion before an influx of particles associated with afternoon upslope winds.

While the SV-OOA factor is lower in general, it is more variable (average $= 1.51 \pm 1.63 \, \mu g \, m^{-3}$); the SV-OOA timeline is punctuated by longer duration, low amplitude concentration increases similar to (and often accompanied by) LV-OOA increases, but short, high-amplitude (4–10 times average, max $= 64 \, \mu g \, m^{-3}$) periods also commensurate with increasing BBOA as discussed above. Like LV-OOA, SV-OOA has two modes in the diurnal average; however, the evening increase is more pronounced than that of LV-OOA (from misallocation of BBOA, as discussed above). SV-OOA is correlated with ammonium and, more weakly, nitrate (Table 2), suggesting influence from urban areas and/or agriculture.

The BBOA factor is generally very low (average $0.46 \pm 0.21 \, \mu g \, m^{-3}$), but has brief (∼1–2 h), higher-concentration episodes; these events occur in the evenings and the occasional afternoon, producing a consistent diurnal mode at ∼22:00 LST commensurate with nighttime campfires at adjacent summer camps and an outlier-driven mean increase at ∼16:00 LST (Fig. 4, High Peak Camp manager Russ Chandler, personal communication,

9 September 2012). BBOA is not correlated with other AMS-determined aerosol components or 17 min PILS-IC potassium ($r^2 = 0.01$); however, the K^+ timeline periodically tracks BBOA. Because K^+ is emitted mainly during the fire flaming phase (versus smoldering), it often lacks correlation with anhydrosugar fragments (e.g., m/z 60), which are more consistent biomass burning markers across burn and fuel types (Lee et al., 2010; Sullivan et al., 2008).

PMF factors are mass-spectrally static; to explore the behavior of and variability within each type of OA, periods dominated by a given factor were subjected to elemental, size, and meteorological analyses which will be presented below. "LV-dominated" periods are indicated when [LV] $\geq 2 \cdot$ [SV], "SV-dominated" periods when [SV] > [LV], and "BBOA-dominated" episodes when [BB] $\geq 2 \cdot 0.46 \, \mu g \, m^{-3}$ (twice the average BBOA factor concentration).

3.3 Elemental analysis and organic nitrogen

The ratio of organic mass to organic carbon (OM:OC) averages 1.99 ± 0.16 and indicates highly oxidized OA consistent with other non-urban sites (Aiken et al., 2008; Turpin and Lim, 2001); O : C averages 0.66 ± 0.13 and H : C averages 1.27 ± 0.09. N : C is determined from CHN and CHON fragments, excluding nominally inorganic fragments such as NO_2^+ that may also arise from fragmentation of or-
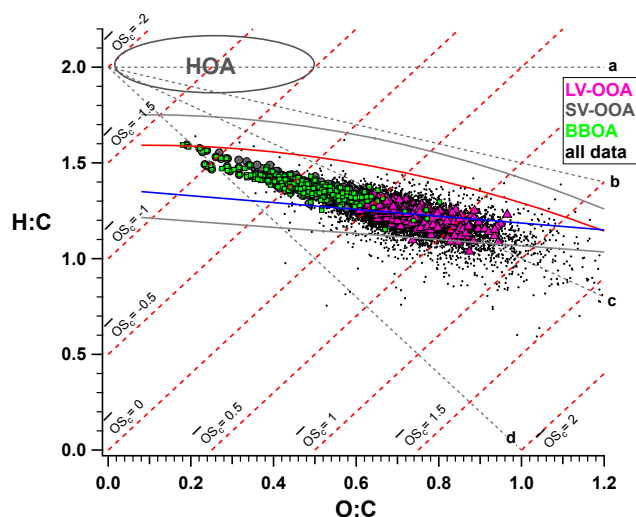
Figure 7. Van Krevelen-triangle diagram for time periods dominated by the given factor (as defined in Sect. 3.3) and for all data points. Estimated oxidation state, $\overline{OS}_c \approx 2 \cdot O : C - H : C$ (Kroll et al., 2011). Red and blue lines indicate the region usually inhabited by ambient data in the *f43* versus *f44* plot; grey lines represent 10 % error. Grey ellipse shows typical HOA values. **(a)** +alcohol/peroxide, $m = 0$; **(b)** carboxylic acid + fragmentation, $m = -0.5$; **(c)** +carboxylic acid (no fragmentation), $m = -1$; **(d)** +ketone/aldehyde, $m = -2$ (Ng et al., 2011).

ganic nitrogen (ON) molecules; N : C averages 0.01 ± 0.01 (max = 0.55).

On the van Krevelen-triangle diagram (Fig. 7) the data position in the apex of the "ambient triangle" space (higher O : C and lower H : C) indicates highly oxidized particles consistent with similar data sets (Ng et al., 2011; Heald et al., 2010); data points are colored by the dominant PMF factor as defined above. SV-OOA- and BBOA-dominated periods occupy similar ranges, while LV-OOA-dominated periods are more oxidized with lower H : C. During BBOA-dominated periods, O : C ranges from ~0.2 to ~0.65, which is a greater range than often observed in the literature (usually ~0.3–0.4, Aiken et al., 2007, 2008; Heringa et al., 2012); the higher maximum degree of oxygenation may arise from the ubiquity of OOA at the site and/or from additional partitioning of oxidized organics onto the new biomass burning particles. The total data set also demonstrates consistent high oxidation (i.e., there are no points in the HOA/POA region of the graph indicated by a grey ellipse). The overlap in van Krevelen space between data points from high-concentration LV- and SV-OOA episodes and the concomitance of SV- and LV-OOA time series ($r^2 = 0.59$) suggest that, *purely in terms of oxidation*, SV- and LV-OOA are somewhat arbitrary delineations between air masses whose aerosol oxidation state varies continuously. However, the different inorganic mixtures (and particle sizes, Sect. 3.4) associated with LV-OOA and SV-OOA validate treating them separately. Linear re-

gressions of O : C/H : C are sometimes used to investigate oxidation mechanisms (Heald et al., 2010). While the reaction mechanisms producing these slopes are best constrained when observing air masses isolated during reaction, a doubtful assumption for this lengthy ambient data set, these values are provided for reference in the supplement.

Quantification of organic nitrogen from AMS data is prevented by fragmentation of ON to nominally inorganic fragments (NO_n^+), the inconsistency of this fragmentation between instruments, and the vast array of possible ON parent compounds in ambient particles (Farmer et al., 2010). However, a lower bound on organic nitrogen mass can be estimated using $ON_{min} = (Org/OM:OC)*N : C*(14/12)$, where Org is total organic mass; ON mass may be underestimated using this method because N : C includes only N from CHON and CHN fragments, disregarding NO_n^+ and/or NH_n^+ produced by ON fragmentation. ON_{min} is small and comprised mostly of CHN fragments (max = 1.04 μg m^{-3}, average = 0.02 ± 0.02 μg m^{-3}). The few, modest ON_{min} events are accompanied by BBOA (although not all BBOA increases are accompanied by ON_{min}) and total nitrate with no commensurate sulfate or ammonium increases (Fig. 8); ON such as nitrophenols (Iinuma et al., 2007), urea (Mace et al., 2003), nitriles, and amines/amides (Simoneit et al., 2003) have been associated with biomass burning in the literature. Although the half-width/half-max fitting rule was always maintained, CHN fragments are often neighbor to larger organic fragment peaks, which generally complicates identification or quantification of the smaller peak; however, our assertion that these fragments represent real CHN content is supported by contemporaneous, co-located filter-based measurements of water-soluble organic nitrogen, which was enhanced during biomass-burning episodes and contained organic bases, as observed here (Benedict, 2012). Though fragmentation in the AMS precludes identification of parent organic molecules, series of CHN fragments at m/z 30 and 58 (with additional peaks at m/z 72, 86, and 100) have been observed in 70eV mass spectra from laboratory and field aerosols with amine content (Murphy et al., 2007; Silva et al., 2008); CH_4N^+ (m/z 30) may result from amine rearrangement after electron impact ionization (Murphy et al., 2007). Here, prominent CHN fragments are noted at m/z 30, 41, 53, 58, 63, 67, 77, 79, 81, 91, and 95 and are organized into the wave pattern often seen in organic spectra (m/z 53, 67, 81, and 95; Series 1 in Fig. 9), which arises from the tendency of organic molecules to lose CH_2 groups sequentially during fragmentation and results in peaks separated by 14 amu. Empirical formulae at m/z 53, 67, 81, and 95 belong overwhelmingly to nitrile and/or pyrrole (heterocyclic) molecules, suggesting that these are (or fragment from) important ON compounds in the local particulate matter; however, because a mixture of amine compounds is possible, molecular structure cannot be determined through fragmentation ratios. Fragments at m/z 63, 77, and 91 form another methylene-subtraction series (Series 2, Fig. 9) for which
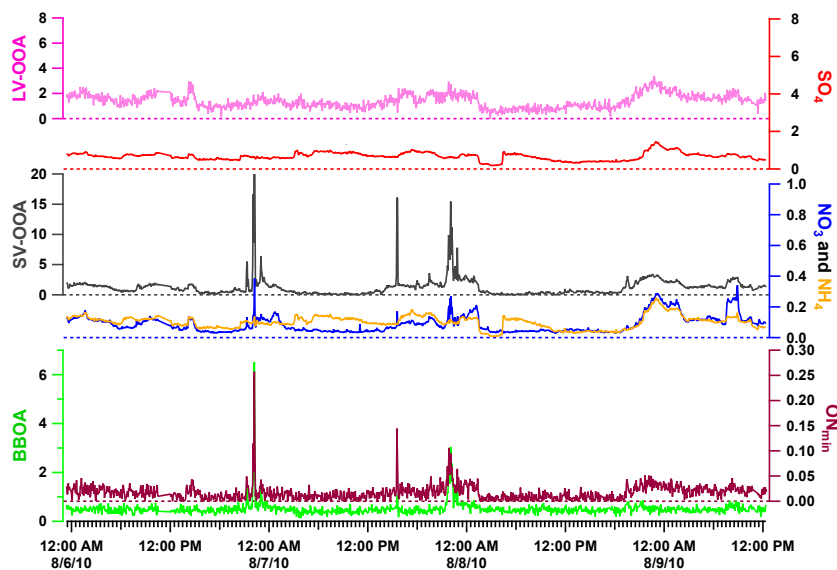
Figure 8. Time series showing select elevated-ON_{min} periods with inorganics and other organic factors.
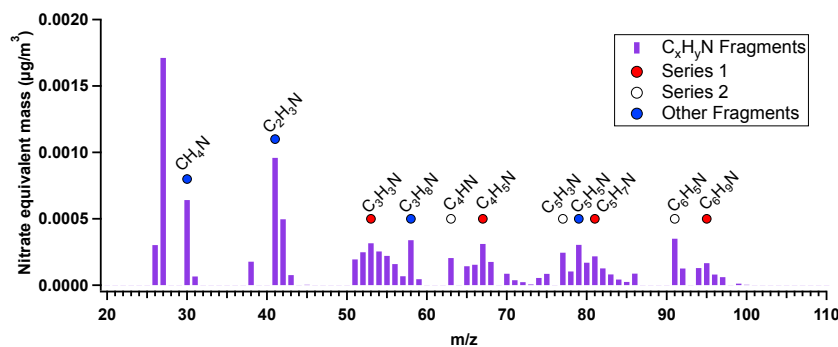

Figure 9. Study-average mass spectrum of CHN fragments.

empirical formulae also suggest nitriles and/or heterocyclic compounds, including pyridine, which is often used to stabilize agricultural fertilizers and is produced in small amounts in biomass burning (McKenzie et al., 1995).

This CHN series, while not found in the literature, is similar to fragments observed in a similar high-altitude site near Grand Teton National Park (m/z 30, 41, 55, 58, 67, 79, 91; Schurman, 2014). The average CHN mass spectrum for elevated-ON_{min} periods (not shown) has a higher CHN signal than the total average, LV-OOA, and SV-OOA spectra but no appreciable difference in fragment patterns, indicating a concentration increase but likely minimal change in CHN composition. The concurrence of increases in ON_{min} and BBOA suggests that ON content, and especially nitrile and/or heteroaromatics, is enhanced in biomass burning plumes. Although CHON fragments (nominally "organonitrates") were fit in the high-resolution analysis, they contained very little mass and no clear fragmentation patterns.

3.4 Particle size

While low particle concentrations and therefore signal prevent continuous size determination for many observed species (notably inorganics), size determination of marker m/z and time periods heavily dominated by a given organic factor can elucidate "average" particle behavior and perhaps atmospheric processing as discussed below. Lognormal fits of average aerosol component mass size distributions allow better statistical comparison of factor-dominated periods and were constructed using the Igor fitting algorithm; lognormal fits also allow size mode estimation in species such as ammonium and nitrate that suffer from lower signal:noise in the raw size distributions.

High-LV-OOA events have larger particles (∼380 nm geometric mean diameter) than SV-OOA episodes (∼300 nm), while BBOA may be slightly smaller (∼280 nm; Fig. 10). As indicated by σ_g (the geometric sd), LV-OOA events are also more monodisperse than SV-OOA; the tendency of condensation and coagulation during oxidation to make particles
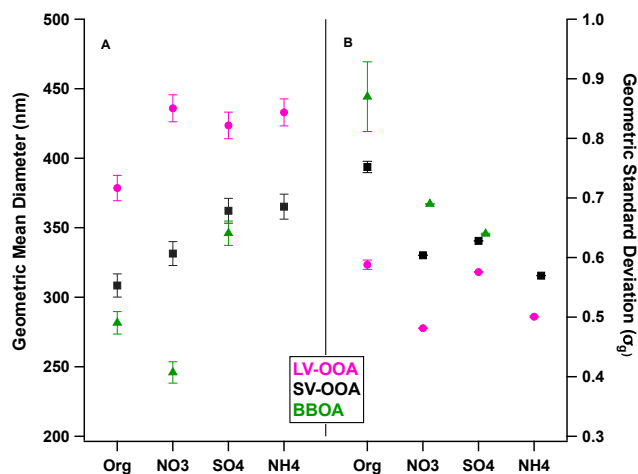
Figure 10. (a) Geometric mean diameter of the log normal mass size distribution fit for the indicated species or total organics for the average of time periods dominated by the color-designated organic factor; error bars are estimations of size-dependent PToF error, compounding chopper broadening and calibration-particle size standard deviation (Supplement). **(b)** Geometric standard deviation of the lognormal fit, with error bars equaling the reduced chi-squared value. Ammonium concentrations were too low during BBOA events for size determination.

larger and more monodisperse suggests that the OOA factors spend time in transit from their source (Seinfeld and Pandis, 2006) and, further, that LV-OOA particles undergo more oxidative processing than SV-OOA particles, as mean radius is observed to increase continuously with ageing (Reid et al., 2005).

The similar size distributions and time series of LV-OOA, ammonium, and sulfate suggest that an internal mixture of these components is common. While SV-OOA and LV-OOA are often coincident, SV-OOA-dominated periods feature smaller particle sizes and a correlation with ammonium nitrate. As mentioned earlier, differences in atmospheric processing of the given components may lead to these distinct mixtures. SV-OOA and ammonium nitrate, all semivolatile species, may arise in the particle phase through condensation of vapors. In contrast, the correlation between LV-OOA and sulfate suggests a possible common aqueous production route. Size distributions of cloud/fog-processed particles tend to be larger than observed here (Hering and Friedlander, 1982; Meng and Seinfeld, 1994), but many of these studies feature heavy, prolonged cloud/fog cover, meteorology, and chemistry (e.g., higher aerosol precursor concentrations), which may differ from brief convective cloud processing in the Front Range. Aqueous reactions in wetted particles are also feasible; the deliquescence relative humidity of mixed ammonium sulfate-organic particles is ~ 30–70% (depending on organic fraction and type) and the ambient surface RH varied from 4 to 100% during this study with an average of $59 \pm 31\%$ (Smith et al., 2012; Takahama et

al., 2007). These RH values are consistent with the historical July–August average RH of $\sim 50\%$, based on monthly-average data (during 1991–2012, CIRA, 2013).

BBOA events are smaller and more polydisperse than other organic factors, higher in amplitude, and not coincident with inorganic species, reflecting a fresher, local particle population given less time to grow by condensation and/or coagulation. With an average organic mode of ~ 280 nm, the biomass burning aerosol at this site is consistent with fresh BB plumes from temperate forests, which range in volume mean diameter from 86 to 300 nm (volume and mass distributions being analogous assuming constant density; Reid et al., 2005 and references therein). Two-dimensional time and size images for some BBOA events at RMNP (not shown) reveal growth of total organics from 100 to 200 nm to ~ 350 nm over the course of the event, consistent with observations in the literature and explained by rapid coagulation and condensation (Adler et al., 2011). The level of oxidation (average $f44 = 0.09 \pm 0.02$ during BB-dominated periods) is consistent with literature SV-OOA; together, the relatively large size (in comparison to some biomass combustion, e.g., mode $= 100$ nm in Adler et al., 2011, though mode may vary with burn type) and advanced oxidation may be explained by the presence of background OOA and/or rapid condensation of semivolatile VOCs onto the increased particle surface area provided by the BB plume.

3.5 Source/transport analysis

The particle composition and size data indicate that oxidized organic aerosol is mixed in varying combinations with inorganic anthropogenic tracers nitrate, sulfate, and ammonium. The level of oxidation argues for prolonged reaction time in the atmosphere; also, limited local habitation precludes high local emissions of inorganic anthropogenic tracers. Together, these suggest transported, anthropogenically influenced OOA particles, which could arise from either anthropogenic OA and SOA precursors, and/or anthropogenic OA and oxidation products of biogenic organics, such as BVOC oxidation in the presence of NO_x (Kiendler-Scharr et al., 2009).

Correlations between secondary OA mass and temperature may indicate which precursors and mechanisms are at play: in many urban/downwind ambient observations, a negative correlation arises from thermodynamically driven partitioning effects, but in heavily forested areas, increased SOA-precursor BVOC emissions from increasing temperature can overwhelm thermodynamic partitioning reduction, causing an overall increase in secondary mass (Leaitch et al., 2011). These studies are usually episode-focused and establish the connectivity of the measured air masses using meteorology and anthropogenic trace gases; at Rocky Mountain, the average relationship between temperature and SOA concentration is determined for periods with upslope and downslope winds. Concentrations of LV-OOA, SV-OOA, SOA (defined

here as LV + SV), and BBOA have no relationship with ambient temperature during either upslope or downslope winds ($r^2 = 0.00$, $m = 0.00$); this could (a) indicate a balance, on average, between thermodynamic partitioning and BVOC precursor emission effects on SOA mass, and/or (b) be a product of the inconsistent lag between wind direction and concentration changes (see below).

Fragmentation within the AMS prevents the molecular specificity needed to determine which of these mechanisms is at play. However, co-located carbon isotope work conducted in a year with total burned area and fire contributions to surface $PM_{2.5}$ similar to those herein indicates that $\sim88\%$ of summer $PM_{2.5}$ carbon is contemporary (Schichtel et al., 2008; Val Martin et al., 2013). From the PMF factors, biomass burning OA (which contains contemporary carbon) contributes a study average of $\sim11\%$ of submicron OC. Thus, biomass burning does not appear to provide all of the observed contemporary C. This suggests that biogenic VOCs may contribute substantially to local OA formation. Levin et al. (2012) described particle growth from condensation of organics in summer at a similar forested Colorado site; concomitant size increase and κ (hygroscopicity parameter) decrease during particle formation events is an indicator of organic condensation.

Associating meteorology with component concentrations and diurnal patterns supports these source indications. Surface winds are funneled by the valley topography and are predominantly down-valley from the WNW (48 %) or up-valley from the SE (16 %); this pattern is consistent interannually, with similar wind roses produced by data from 1995 to 2005 (Malm et al., 2009a). Raw and directionally averaged concentrations of aerosol components plotted against surface wind direction over sixteen $22°30'$ wind direction bins are shown with CPFs in Fig. 11. High inorganic concentrations are associated with local SE winds indicating upvalley movement from the Front Range and are very similar in both CPF value and meteorological association to co-located $PM_{2.5}$ measurements (note that CPFs are multiplied by 10 to share a scale with concentration; Benedict et al., 2013b). CPFs for OOA factors also have an association with SE winds, and higher average concentrations are associated with S-SE winds for all components (including BBOA, though from a different source; see below). However, unlike organics, OOA factors also have above-average concentrations associated with NW winds (though not above the CPF threshold). This may indicate regional OOA content (i.e., background organics), possibly aged biogenic SOA from forest emissions, which could originate from the west and be unassociated with Front Range emissions; aqueous processing in orographic clouds arising from westerly flow over the mountains could also contribute to this OOA.

High BBOA concentrations are usually associated with NW or SW-to-S surface winds. The closest campfire source is ~200 m WNW of the sampling site; the shorter transport (and therefore dilution) time may explain the higher concen-
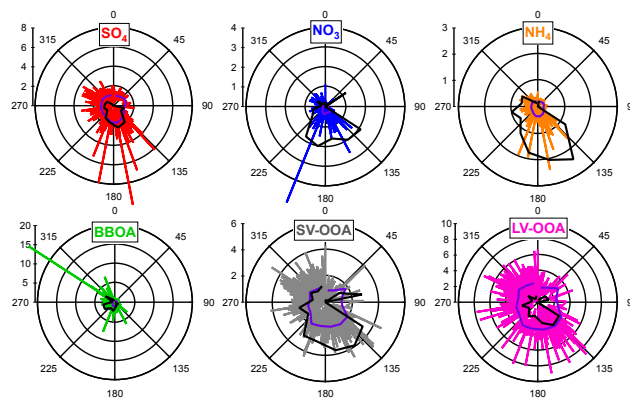

Figure 11. 1 h average concentrations (μg m^{-3}) of organic aerosol types with surface wind direction. Raw data are colored by species, average concentrations over the sixteen $22°30'$ wind direction bins are shown in purple, and black lines indicate the conditional probability function (CPF multiplied by 10).

trations in BBOA events from the WNW. Three other camps are placed ~0.5–1 km due south; the increased number and distance of the fires explains the higher average but lower maximum concentrations associated with SW-to-S winds.

3.6 Episode analysis

The aerosol characteristics summarized previously are demonstrated in a series of alternating high- and low-concentration periods during 7–11 July that clearly show the transport of OOA and inorganics by SE surface winds (Fig. 12). Initiation of SE flow is followed by marked concentration increases after ~3 h, suggesting a 3 h transport time between the Front Range and RMNP during this period. A similar lag applies between down-valley flow initiation and concentration decreases; the fact that 1–3 h offsets did not improve correlation between wind direction and species concentrations indicates that transport time is, not surprisingly, variable. The abrupt decreases in all components' concentrations following NW wind initiation reveals the relative cleanliness of the air coming over the mountains during these periods. Lastly, note the apparent discrepancy during period A, where $\sim$NW winds are accompanied by sharp spikes in SV-OOA; this is thought to be an entanglement of BBOA mass with SV-OOA (Sect. 3.2) as evidenced by the short, high-amplitude concentration increase, enhancement of m/z 60 in the mass spectrum (not shown), and lack of attendant increase in anthropogenic inorganics. This hypothesis is corroborated by an increase in BBOA in the recombinant-factor PMF analysis and the NW placement of the campfire source (as winds are from the north).
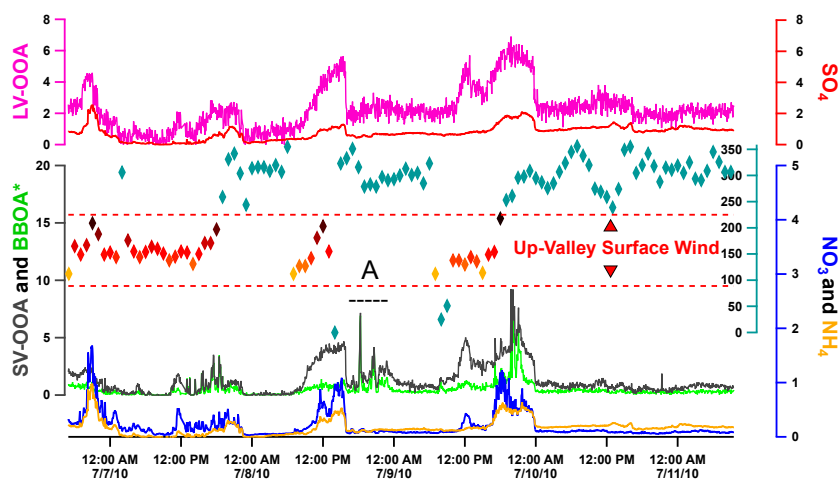
Figure 12. Timeline of species and relevant organic factor concentrations for 7–11 July 2010, plotted with 1 h surface wind direction at the site (diamonds). Wind directions 90 through 180 degrees denote up-valley winds and are demarcated by dashed red lines and warm-colored diamonds. BBOA* is calculated using the six-factor PMF reconstructions outlined in the Supplement.

4 Summary and conclusions

The ambient submicron aerosol at the RMNP ROMO site during 2 July–31 August 2010 is low in average concentration (total average $PM_1 = 5.13 \pm 2.72\,\mu g\,m^{-3}$), dominated by highly oxidized organics (LV-OOA and SV-OOA), and punctuated by short biomass burning (BBOA) episodes. Mixtures of LV-OOA with ammonium sulfate and SV-OOA with ammonium nitrate are indicated by consistent size distributions and time series correlation. Inorganic species (nitrate, sulfate, and ammonium) are established anthropogenic emission tracers for which no strong local sources are apparent; high inorganic concentrations are concurrent with southeasterly surface winds that indicate upslope flow from the Front Range. A biogenic contribution, possibly from oxidation of BVOCs as Front Range oxidant-rich pollution plumes are transported over the forest, is suggested by the fact that contemporary carbon contributed by local biomass burning may not account for total contemporary carbon at the site (though data sets are not contemporaneous; Schichtel et al., 2008). Organic nitrogen fragments are associated with BBOA and may indicate amine, nitrile, and/or heterocyclic aromatic content but are low in mass (omitting nominally inorganic fragments from ON calculations); BBOA is not correlated with any measured inorganic species.

Transport of oxidized organic aerosols from the Front Range is indicated by advanced oxidation and relative monodispersity (both indicative of ageing), association with inorganic anthropogenic tracers, and concentration correlation with surface upslope flow from the urban and agriculture emissions-rich Front Range; the presence of sulfate, periodic high relative humidity and cloud cover, larger particle sizes, and advanced oxidation of the LV-OOA suggest possible contributions from aqueous processing, while growth by va-

por condensation is more likely for SV-OOA/ammonium nitrate particles. A local BBOA source is suggested by biomass combustion markers (m/z 60 and 73) limited to brief, high-concentration, polydisperse events (suggesting fresh combustion emission), association with local S or NW winds consistent with campfire locations, and an unequivocal diurnal maximum at 22:00 LST, when campfires were set at adjacent summer camps.

Lastly, the particle characteristics and sources determined here appear to be typical of summer conditions at the Rocky Mountain site, based on the historical meteorological patterns, IMPROVE (total $PM_{2.5}$, sulfate, nitrate, ammonium, and OC), PILS-IC ($PM_{2.5}$ sulfate, nitrate, and ammonium), filter ($PM_{2.5}$ sulfate, nitrate, and ammonium), and fire (burned area, contribution to surface $PM_{2.5}$) data analyzed here.

References

Adler, G., Flores, J. M., Abo Riziq, A., Borrmann, S., and Rudich, Y.: Chemical, physical, and optical evolution of biomass burning aerosols: a case study, Atmos. Chem. Phys., 11, 1491–1503, doi:10.5194/acp-11-1491-2011, 2011.

Aiken, A. C., DeCarlo, P. F., and Jimenez, J. L.: Elemental analysis of organic species with electron ionization high-resolution mass spectrometry, Anal. Chem., 79, 8350–8358, doi:10.1021/ac071150w, 2007.

Aiken, A. C., Decarlo, P. F., Kroll, J. H., Worsnop, D. R., Huffman, J. A., Docherty, K. S., Ulbrich, I. M., Mohr, C., Kimmel, J. R., Sueper, D., Sun, Y., Zhang, Q., Trimborn, A., Northway, M., Ziemann, P. J., Canagaratna, M. R., Onasch, T. B., Alfarra, M. R., Prevot, A. S. H., Dommen, J., Duplissy, J., Metzger, A., Baltensperger, U., and Jimenez, J. L.: O/C and OM/OC ratios of primary, secondary, and ambient organic aerosols with high-resolution time-of-flight aerosol mass spectrometry, Environ. Sci. Technol., 42, 4478–4485, 2008.

Alfarra, M. R., Prevot, A. S. H., Szidat, S., Sandradewi, J., Weimer, S., Lanz, V. A., Schreiber, D., Mohr, M., and Baltensperger, U.: Identification of the mass spectral signature of organic aerosols from wood burning emissions, Environ. Sci. Technol., 41, 5770–5777, 2007.

Allan, J. D., Jimenez, J. L., Williams, P. I., Alfarra, M. R., Bower, K. N., Jayne, J. T., Coe, H., and Worsnop, D. R.: Quantitative sampling using an Aerodyne aerosol mass spectrometer 1. Techniques of data interpretation and error analysis, J. Geophys. Res., 108, 1–10, doi:10.1029/2002JD002358, 2003.

Baron, J. S., Rueth, H. M., Wolfe, A. M., Nydick, K. R., Allstott, E. J., Minear, J. T., and Moraska, B.: Ecosystem responses to nitrogen deposition in the Colorado Front Range, Ecosystems, 3, 352–368, 2000.

Barth, M. C., Rasch, P. J., Kiehl, J. T., Benkovitz, C. M., and Schwartz, S. E.: Sulfur chemistry in the National Center for Atmospheric Research Community Climate Model: Description, evaluation, features, and sensitivity to aqueous chemistry, J. Geophys. Res., 105, 1387, doi:10.1029/1999JD900773, 2000.

Beem, K. B., Raja, S., Schwandner, F. M., Taylor, C., Lee, T., Sullivan, A. P., Carrico, C. M., McMeeking, G. R., Day, D., Levin, E., Hand, J., Kreidenweis, S. M., Schichtel, B., Malm, W. C., and Collett, J. L.: Deposition of reactive nitrogen during the Rocky Mountain Airborne Nitrogen and Sulfur (RoMANS) study., Environ. Pollut., 158, 862–872, doi:10.1016/j.envpol.2009.09.023, 2010.

Benedict, K. B.: Observations of Atmospheric Reactive Nitrogen Species and Nitrogen Deposition in the Rocky Mountains, Colorado State University, Fort Collins, CO, 2012.

Benedict, K. B., Carrico, C. M., Kreidenweis, S. M., Schichtel, B., Malm, W. C., and Collett, J. L.: A seasonal nitrogen deposition budget for Rocky Mountain National Park, Ecol. Appl., 23, 1156–1169, doi:10.1890/12-1624.1, 2013a.

Benedict, K. B., Day, D., Schwandner, F. M., Kreidenweis, S. M., Schichtel, B., Malm, W. C., and Collett, J. L.: Observations of atmospheric reactive nitrogen species in Rocky Mountain National Park and across northern Colorado, Atmos. Environ., 64, 66–76, doi:10.1016/j.atmosenv.2012.08.066, 2013b.

Bossert, J. E. and Cotton, W. R.: Regional-Scale Flows in Mountainous Terrain. Part I: A Numerical and Observational Comparison. Monthly Weather Review, 122, 1449–1471, doi:10.1175/1520-0493(1994)122<1449:RSFIMT>2.0.CO;2, 1994.

Chan, Y., Hawas, O., Hawker, D., Vowles, P., Cohen, D. D., Stelcer, E., Simpson, R., Golding, G., and Christensen, E.: Using multiple type composition data and wind data in PMF analysis to apportion and locate sources of air pollutants, Atmos. Environ., 45, 439–449, doi:10.1016/j.atmosenv.2010.09.060, 2011.

Chen, Q., Farmer, D. K., Schneider, J., Zorn, S. R., Heald, C. L., Karl, T. G., Guenther, A., Allan, J. D., Robinson, N., Coe, H., Kimmel, J. R., Pauliquevis, T., Borrmann, S., Pöschl, U., Andreae, M. O., Artaxo, P., Jimenez, J. L., and Martin, S. T.: Mass spectral characterization of submicron biogenic organic particles in the Amazon Basin, Geophys. Res. Lett., 36, L20806, doi:10.1029/2009GL039880, 2009.

CIRA: VIEWS Database, available at: from http://views.cira.colostate.edu/web/ (last access: 22 January 2014), 2013.

Corrigan, A. L., Russell, L. M., Takahama, S., Äijälä, M., Ehn, M., Junninen, H., Rinne, J., Petäjä, T., Kulmala, M., Vogel, A. L., Hoffmann, T., Ebben, C. J., Geiger, F. M., Chhabra, P., Seinfeld, J. H., Worsnop, D. R., Song, W., Auld, J., and Williams, J.: Biogenic and biomass burning organic aerosol in a boreal forest at Hyytiälä, Finland, during HUMPPA-COPEC 2010, Atmos. Chem. Phys., 13, 12233–12256, doi:10.5194/acp-13-12233-2013, 2013.

Decarlo, P. F., Kimmel, J. R., Trimborn, A., Northway, M. J., Jayne, J. T., Aiken, A. C., Gonin, M., Fuhrer, K., Horvath, T., Docherty, K. S., Worsnop, D. R., and Jimenez, J. L.: Field-deployable, high-resolution, time-of-flight aerosol mass spectrometer, Anal. Chem., 78, 8281–8289, doi:10.1021/ac061249n, 2006.

Echalar, F., Gaudichet, A., Cachier, H., and Artaxo, P.: Aerosol emissions by tropical forest and savanna biomass burning: Characteristic trace elements and fluxes, Geophys. Res. Lett., 22, 3039, doi:10.1029/95GL03170, 1995.

Farmer, D. K., Matsunaga, A., Docherty, K. S., Surratt, J. D., Seinfeld, J. H., Ziemann, P. J., and Jimenez, J. L.: Response of an aerosol mass spectrometer to organonitrates and organosulfates and implications for atmospheric chemistry, P. Natl. Acad. Sci., 107, 6670–6675, 2010.

Gebhart, K. A., Schichtel, B. A., Malm, W. C., Barna, M. G., Rodriguez, M. A., and Collett, J. L.: Back-trajectory-based source apportionment of airborne sulfur and nitrogen concentrations at Rocky Mountain National Park, Colorado, USA, Atmos. Environ., 45, 621–633, doi:10.1016/j.atmosenv.2010.10.035, 2011.

Hand, J. L., Schichtel, B. A., Pitchford, M., Malm, W. C., and Frank, N. H.: Seasonal composition of remote and urban fine particulate matter in the United States, J. Geophys. Res., 117, D05209, doi:10.1029/2011JD017122, 2012.

Heald, C. L., Kroll, J. H., Jimenez, J. L., Docherty, K. S., DeCarlo, P. F., Aiken, A. C., Chen, Q., Martin, S. T., Farmer, D. K., and Artaxo, P.: A simplified description of the evolution of organic aerosol composition in the atmosphere, Geophys. Res. Lett., 37, L08803, doi:10.1029/2010GL042737, 2010.

Hering, S. V. and Friedlander, S. K.: Origins of aerosol sulfur size distributions in the Los Angeles basin, Atmos. Environ., 16, 2647–2656, doi:10.1016/0004-6981(82)90346-8, 1982.

Heringa, M. F., DeCarlo, P. F., Chirico, R., Tritscher, T., Clairotte, M., Mohr, C., Crippa, M., Slowik, J. G., Pfaffenberger, L., Dommen, J., Weingartner, E., Prévôt, A. S. H., and Baltensperger, U.: A new method to discriminate secondary organic aerosols from different sources using high-resolution aerosol mass spectra, Atmos. Chem. Phys., 12, 2189–2203, doi:10.5194/acp-12-2189-2012, 2012.

Iinuma, Y., Brüggemann, E., Gnauk, T., Müller, K., Andreae, M. O., Helas, G., Parmar, R., and Herrmann, H.: Source characterization of biomass burning particles: The combustion of selected European conifers, African hardwood, savanna grass, and German and Indonesian peat, J. Geophys. Res., 112, D08209, doi:10.1029/2006JD007120, 2007.

Jimenez, J. L., Canagaratna, M. R., Donahue, N. M., Prevot, A. S. H., Zhang, Q., Kroll, J. H., DeCarlo, P. F., Allan, J. D., Coe, H., Ng, N. L., Aiken, A. C., Docherty, K. S., Ulbrich, I. M., Grieshop, A. P., Robinson, A. L., Duplissy, J., Smith, J. D., Wilson, K. R., Lanz, V. A., Hueglin, C., Sun, Y. L., Tian, J., Laaksonen, A., Raatikainen, T., Rautiainen, J., Vaattovaara, P., Ehn, M., Kulmala, M., Tomlinson, J. M., Collins, D. R., Cubison, M. J., Dunlea, E. J., Huffman, J. A., Onasch, T. B., Alfarra, M. R., Williams, P. I., Bower, K. N., Kondo, Y., Schneider, J., Drewnick, F., Borrmann, S., Weimer, S., Demerjian, K. L., Salcedo, D., Cottrell, L. D., Griffin, R. J., Takami, A., Miyoshi, T., Hatakeyama, S., Shimono, A., Sun, J. Y., Zhang, Y. M., Dzepina, K., Kimmel, J. R., Sueper, D., Jayne, J. T., Herndon, S. C., Trimborn, A. M., Williams, L. R., Wood, E. C., Middlebrook, A. M., Kolb, C. E., Baltensperger, U., and Worsnop, D. R.: Evolution of organic aerosols in the atmosphere, Science New York, NY, 326, 1525–1529, doi:10.1126/science.1180353, 2009.

Kiendler-Scharr, A., Zhang, Q., Hohaus, T., Kleist, E., Mensah, A., Mentel, T. F., Spindler, C., Uerlings, R., Tillmann, R., Wildt, J.: Aerosol mass spectrometric features of biogenic SOA: observations from a plant chamber and in rural atmospheric environments, Environ. Sci. Technol., 43, 8166–8172, doi:10.1021/es901420b, 2009.

Kim, E. and Hopke, P. K.: Comparison between Conditional Probability Function and Nonparametric Regression for Fine Particle Source Directions, Atmos. Environ., 38, 4667–4673, doi:10.1016/j.atmosenv.2004.05.035, 2004.

Kroll, J. H., Donahue, N. M., Jimenez, J. L., Kessler, S. H., Canagaratna, M. R., Wilson, K. R., Altieri, K. E., Mazzoleni, L. R., Wozniak, A. S., Bluhm, H., Mysak, E. R., Smith, J. D., Kolb, C. E., and Worsnop, D. R.: Carbon oxidation state as a metric for describing the chemistry of atmospheric organic aerosol, Nature Chem., 3, 133–139, doi:10.1038/nchem.948, 2011.

Lanz, V. A., Alfarra, M. R., Baltensperger, U., Buchmann, B., Hueglin, C., and Prévôt, A. S. H.: Source apportionment of submicron organic aerosols at an urban site by factor analytical modelling of aerosol mass spectra, Atmos. Chem. Phys., 7, 1503–1522, doi:10.5194/acp-7-1503-2007, 2007.

Leaitch, W. R., Macdonald, A. M., Brickell, P. C., Liggio, J., Sjostedt, S. J., Vlasenko, A., Bottenheim, J. W., Huang, L., Li, S.-M., Liu, P. S. K., Toom-Sauntry, D., Hayden, K. A., Sharma, S., Shantz, N. C., Wiebe, H. A., Zhang, W., Abbatt, J. P. D., Slowik, J. G., Chang, R. Y. W., Russell, L. M., Schwartz, R. E., Takahama, S., Jayne, J. T., and Ng, N. L.: Temperature response of the submicron organic aerosol from temperate forests, Atmos. Environ., 45, 6696–6704, doi:10.1016/j.atmosenv.2011.08.047, 2011.

Lee, T., Sullivan, A. P., Mack, L., Jimenez, J. L., Kreidenweis, S. M., Onasch, T. B., Worsnop, D. R., Malm, W. C., Wold, C. E., Hao, W. M., and Collett, J. L.: Chemical Smoke Marker Emissions During Flaming and Smoldering Phases of Laboratory Open Burning of Wildland Fuels, Aerosol Sci. Technol., 44, 2635–2643, doi:10.1080/02786826.2010.499884, 2010.

Lelieveld, J. and Heintzenberg, J.: Sulfate Cooling Effect on Climate Through In-Cloud Oxidation of Anthropogenic SO_2, Science, New York, NY, 258, 117–20, doi:10.1126/science.258.5079.117, 1992.

Levin, E. J. T., Kreidenweis, S. M., McMeeking, G. R., Carrico, C. M., Collett Jr., J. L., and Malm, W. C.: Aerosol physical, chemical and optical properties during the Rocky Mountain Airborne Nitrogen and Sulfur study, Atmos. Environ., 43, 1932–1939, doi:10.1016/j.atmosenv.2008.12.042, 2009.

Levin, E. J. T., Prenni, A. J., Petters, M. D., Kreidenweis, S. M., Sullivan, R. C., Atwood, S. A., Ortega, J., DeMott, P. J., and Smith, J. N.: An annual cycle of size-resolved aerosol hygroscopicity at a forested site in Colorado, J. Geophys. Res., 117, D06201, doi:10.1029/2011JD016854, 2012.

Mace, K. A., Artaxo, P., and Duce, R. A.: Water-soluble organic nitrogen in Amazon Basin aerosols during the dry (biomass burning) and wet seasons, J. Geophys. Res., 108, 4512, doi:10.1029/2003JD003557, 2003.

Malm, W. C., Barna, M. G., Beem, K. B., Carrico, C. M., Collett Jr., J. L., Day, D. E., Gebhart, K. A., Hand, J. L., Kreidenweis, S. M., Lee, T., Levin, E.J.T., McDade, C. E., McMeeking, G. R., Molenar, J. V., Raja, S., Rodriguez, M. A., Schichtel, B. A., Schwandner, F. M., Sullivan, A. P., and Taylor, C.: Rocky Mountain Atmospheric Nitrogen and Sulfur Study, Fort Collins, CO, Cooperative Institute for Research in the Atmosphere, 2009a.

Malm, W. C., McMeeking, G. R., Kreidenweis, S. M., Levin, E. J. T., Carrico, C. M., Day, D. E., Collett Jr., J. L., Lee, T., Sullivan, A. P., and Raja, S.: Using high time resolution aerosol and number size distribution measurements to estimate atmospheric extinction, J. Air Waste Manage. Assoc., 59, 1049–1060, 2009b.

McKenzie, L. M., Hao, W. M., Richards, G. N., and Ward, D. E.: Measurement and modeling of air toxins from smoldering combustion of biomass, Environ. Sci. Technol., 29, 2047–2054, doi:10.1021/es00008a025, 1995.

Meng, Z. and Seinfeld, J. H.: On the Source of the Submicrometer Droplet Mode of Urban and Regional Aerosols, Aerosol Sci. Technol., 20, 253–265, doi:10.1080/02786829408959681, 1994.

Murphy, S. M., Sorooshian, A., Kroll, J. H., Ng, N. L., Chhabra, P., Tong, C., Surratt, J. D., Knipping, E., Flagan, R. C., and Seinfeld, J. H.: Secondary aerosol formation from atmospheric reactions of aliphatic amines, Atmos. Chem. Phys., 7, 2313–2337, doi:10.5194/acp-7-2313-2007, 2007.

Ng, N. L., Canagaratna, M. R., Zhang, Q., Jimenez, J. L., Tian, J., Ulbrich, I. M., Kroll, J. H., Docherty, K. S., Chhabra, P. S., Bahreini, R., Murphy, S. M., Seinfeld, J. H., Hildebrandt,

L., Donahue, N. M., DeCarlo, P. F., Lanz, V. A., Prévôt, A. S. H., Dinar, E., Rudich, Y., and Worsnop, D. R.: Organic aerosol components observed in Northern Hemispheric datasets from Aerosol Mass Spectrometry, Atmos. Chem. Phys., 10, 4625–4641, doi:10.5194/acp-10-4625-2010, 2010.

Ng, N. L., Canagaratna, M. R., Jimenez, J. L., Chhabra, P. S., Seinfeld, J. H., and Worsnop, D. R.: Changes in organic aerosol composition with aging inferred from aerosol mass spectra, Atmos. Chem. Phys., 11, 6465–6474, doi:10.5194/acp-11-6465-2011, 2011.

Orsini, D. A., Ma, Y., Sullivan, A. P., Sierau, B., Baumann, K., and Weber, R. J.: Refinements to the particle-into-liquid sampler (PILS) for ground and airborne measurements of water soluble aerosol composition, Atmos. Environ., 37, 1243–1259, 2003.

Paatero, P. and Hopke, P. K.: Discarding or downweighting high-noise variables in factor analytic models, Anal. Chim. Acta, 490, 277–289, doi:10.1016/S0003-2670(02)01643-4, 2003.

Paatero, P. and Tapper, U.: Positive matrix factorization: A non-negative factor model with optimal utilization of error estimates of data values, Environmetrics, 5, 111–126, 1994.

Paatero, P., Hopke, P. K., Song, X.-H., and Ramadan, Z.: Understanding and controlling rotations in factor analytic models, Chemom. Intell. Lab. Syst., 60, 253–264, doi:10.1016/S0169-7439(01)00200-3, 2002.

Parrish, D. D., Hahn, C. H., Fahey, D. W., Williams, E. J., Bollinger, M. J., Hübler, G., Buhr, M. P., Murphy, P. C., Trainer, M., Hsie, E. Y., Liu, S. C., and Fehsenfeld, F. C.: Systematic Variations in the Concentration of NO_x (NO Plus NO_2) at Niwot Ridge, Colorado, J. Geophys. Res., 95, 1817–1836, doi:10.1029/JD095iD02p01817, 1990.

Reid, J. S., Koppmann, R., Eck, T. F., and Eleuterio, D. P.: A review of biomass burning emissions part II: intensive physical properties of biomass burning particles, Atmos. Chem. Phys., 5, 799–825, doi:10.5194/acp-5-799-2005, 2005.

Schichtel, B. A., Malm, W. C., Bench, G., Fallon, S., McDade, C. E., Chow, J. C., and Watson, J. G.: Fossil and contemporary fine particulate carbon fractions at 12 rural and urban sites in the United States, J. Geophys. Res., 113, D02311, doi:10.1029/2007JD008605, 2008.

Schurman, M. I.: Characteristics, Sources, and Formation of Organic Aerosols in the Rocky Mountains. Colorado State University, Fort Collins, Colorado, 2014.

Seinfeld, J. H. and Pandis, S. N.:Atmospheric Chemistry and Physics: From Air Pollution to Climate Change (2nd ed., p. 1232). New York, John Wiley and Sons. New York, New York, USA, 2006.

Silva, P. J., Erupe, M. E., Price, D., Elias, J., Malloy, Q. G. J., Li, Q., Warren, B., and Cocker, D. R.: Trimethylamine as precursor to secondary organic aerosol formation via nitrate radical reaction in the atmosphere, Environ. Sci. Technol., 42, 4689–4696, 2008.

Simoneit, B. R. T., Schauer, J. J., Nolte, C. G., Oros, D. R., Elias, V. O., Fraser, M. P., Rogge, W. F., and Cass, G. R.: Levoglucosan, a tracer for cellulose in biomass burning and atmospheric particles, Atmos. Environ., 33, 173–182, doi:10.1016/S1352-2310(98)00145-9, 1999.

Simoneit, B. R. T., Rushdi, A. I., bin Abas, M. R., and Didyk, B. M.: Alkyl Amides and Nitriles as Novel Tracers for Biomass Burning, Environ. Sci. Technol., 37, 16–21, doi:10.1021/es020811y, 2003.

Smith, M. L., Bertram, A. K., and Martin, S. T.: Deliquescence, efflorescence, and phase miscibility of mixed particles of ammonium sulfate and isoprene-derived secondary organic material, Atmos. Chem. Phys., 12, 9613–9628, doi:10.5194/acp-12-9613-2012, 2012.

Solomon, S., Qin, D., Manning, M., Chen, Z., Marquis, M., Averyt, K. B., Tigora, M., and Miller, H. L.: Climate Change 2007: The Physical Science Basis, in: Fourth Assessment Report of the Intergovernmental Panel on Climate Change, Cambridge, Cambridge University Press, 2007.

Sullivan, A. P., Holden, A. S., Patterson, L. A., McMeeking, G. R., Kreidenweis, S. M., Malm, W. C., Hao, W. M., Wold, C. E., and Collett, J. L.: A method for smoke marker measurements and its potential application for determining the contribution of biomass burning from wildfires and prescribed fires to ambient $PM_{2.5}$ organic carbon, J. Geophys. Res., 113, D22302, doi:10.1029/2008JD010216, 2008.

Sun, J., Zhang, Q., Canagaratna, M. R., Zhang, Y., Ng, N. L., Sun, Y., Jayne, J. T., Zhang, X., Zhang, X., and Worsnop, D. R.: Highly time- and size-resolved characterization of submicron aerosol particles in Beijing using an Aerodyne Aerosol Mass Spectrometer, Atmos. Environ., 44, 131–140, doi:10.1016/j.atmosenv.2009.03.020, 2010.

Sun, Y., Zhang, Q., Macdonald, A. M., Hayden, K., Li, S. M., Liggio, J., Liu, P. S. K., Anlauf, K. G., Leaitch, W. R., Steffen, A., Cubison, M., Worsnop, D. R., van Donkelaar, A., and Martin, R. V.: Size-resolved aerosol chemistry on Whistler Mountain, Canada with a high-resolution aerosol mass spectrometer during INTEX-B, Atmos. Chem. Phys., 9, 3095–3111, doi:10.5194/acp-9-3095-2009, 2009.

Takahama, S., Pathak, R. K., and Pandis, S. N.: Efflorescence Transitions of Ammonium Sulfate Particles Coated with Secondary Organic Aerosol, Environ. Sci. Technol., 41, 2289–2295, doi:10.1021/es0619915, 2007.

Turpin, B. J. and Lim, H.-J.: Species Contributions to $PM_{2.5}$ Mass Concentrations: Revisiting Common Assumptions for Estimating Organic Mass, Aerosol Sci. Technol., 35, 602–610, doi:10.1080/02786820119445, 2001.

Ulbrich, I. M., Canagaratna, M. R., Zhang, Q., Worsnop, D. R., and Jimenez, J. L.: Interpretation of organic components from Positive Matrix Factorization of aerosol mass spectrometric data, Atmos. Chem. Phys., 9, 2891–2918, doi:10.5194/acp-9-2891-2009, 2009.

Ulbrich, I. M., Canagaratna, M. R., Cubison, M. J., Zhang, Q., Ng, N. L., Aiken, A. C., and Jimenez, J. L.: Three-dimensional factorization of size-resolved organic aerosol mass spectra from Mexico City, Atmos. Meas. Tech., 5, 195–224, doi:10.5194/amt-5-195-2012, 2012

Val Martin, M., Heald, C. L., Ford, B., Prenni, A. J., and Wiedinmyer, C.: A decadal satellite analysis of the origins and impacts of smoke in Colorado, Atmos. Chem. Phys., 13, 7429–7439, doi:10.5194/acp-13-7429-2013, 2013.

Weimer, S., Alfarra, M. R., Schreiber, D., Mohr, M., Prévôt, a. S. H., and Baltensperger, U.: Organic aerosol mass spectral signatures from wood-burning emissions: Influence of burning conditions and wood type, J. Geophys. Res., 113, 1–10, doi:10.1029/2007JD009309, 2008.

Xie, Y. and Berkowitz, C. M.: The use of conditional probability functions and potential source contribution functions to

identify source regions and advection pathways of hydrocarbon emissions in Houston, Texas, Atmos. Environ., 41, 5831–5847, doi:10.1016/j.atmosenv.2007.03.049, 2007.

Zhang, Q., Alfarra, M. R., Worsnop, D. R., Allan, J. D., Coe, H., Canagaratna, M. R., and Jimenez, J. L.: Deconvolution and quantification of hydrocarbon-like and oxygenated organic aerosols based on aerosol mass spectrometry, Environ. Sci. Technol., 39, 4938–4952, 2005.

Zhang, Q., Jimenez, J. L., Canagaratna, M. R., Allan, J. D., Coe, H., Ulbrich, I. M., and Worsnop, D. R.: Ubiquity and dominance of oxygenated species in organic aerosols in anthropogenically-influenced Northern Hemisphere midlatitudes, Geophys. Res. Lett., 34, 1–6, doi:10.1029/2007GL029979, 2007.

Zhang, Q., Jimenez, J. L., Canagaratna, M. R., Ulbrich, I. M., Ng, N. L., Worsnop, D. R., and Sun, Y.: Understanding atmospheric organic aerosols via factor analysis of aerosol mass spectrometry: a review, Anal. Bioanal. Chem., 401, 3045–3067, doi:10.1007/s00216-011-5355-y, 2011.

Zhou, L., Hopke, P. K., Stanier, C. O., Pandis, S. N., Ondov, J. M., and Pancras, J. P.: Investigation of the relationship between chemical composition and size distribution of airborne particles by partial least squares and positive matrix factorization, J. Geophys. Res., 110, D07S18, doi:10.1029/2004JD005050, 2005.